Electronic Supplementary Information

Experimental Section

Materials: All reagents used in this work are analytical grade. Polyacrylonitrile (PVP M_w=1300000), polyacrylonitrile (PAN Mw=150000), N,N-Dimethylformamide (DMF), sodium hydroxide (NaOH), Sodium nitrate ($NaNO_3$, 99.0%), Cobaltous nitrate hexahydrate ($Co(NO_3)_2·6H_2O$), Ferric nitrate nonahydrate ($Fe(NO_3)_3·9H_2O$), hydrochloric acid (HCl), ammonium chloride (NH_4Cl)，sulfuric acid (H_2SO_4), were purchased from Kelong chemically(Chengdu, China). sodium nitroferricyanide dihydrate($C_5FeN_6Na_2O·2H_2O$), sodium salicylate($C_7H_5NaO_3$), salicylic acid ($C_7H_6O_3$), trisodium citrate dihydrate ($C_6H_5Na_3O_7·2H_2O$), sodium hypochlorite solution (NaClO), pp-dimethylamino benzaldehyde($C_9H_{11}NO$), 0.8 wt% sulfamic acid solution (H_3NO_3S), were purchased from Aladdin Ltd (Shanghai, China). Nafion solution (5 wt%) was purchased from Sigma-Aldrich Chemical Reagent Co., and Ltd. Deionized water was purified through a Millipore system.

Preparation of catalysts: Carbon nanofibers loaded with different ratios of CoFe alloys prepared by the electrospinning method. Firstly, 0.5 g of PVP and 0.5 g of PAN were dissolved in 10 ml of DMF with stirring for 1 h. Then 1 mmol of $Co(NO_3)_2·6H_2O$ and 1 mmol of $Fe(NO_3)_3·9H_2O$ were added into the above solution with stirring for 24 h at room temperature to form precursor solution. Subsequently, the prepared solution was moved to a syringe with a stainless-steel nozzle. A high-voltage of 20 kV was supplied and the distance between the needle tip and the rotating drum collector is 15 cm. After the spinning was finished, the nanofibers were collected and transferred to a

vacuum oven kept at 80 °C for at least 12 h, in order to remove the moisture in the obtained fabric. The nanofibers were further heated in N_2 atmosphere at 800 °C for 5 h in a tube furnace. The heating and cooling rates were both 2 °C min^{-1}. After calcination, the target catalysts were obtained successfully, denoted as Co_1Fe_1@CNFs. By keeping the content of total metal salts as 2 mmol, adjusting the ratio of CoFe alloy as (Co:Fe=1:9,1:2,2:1,9:1), other conditions were consistent with the above, obtained the carbon nanofibers loaded with different ratios of CoFe alloys, respectively named Co_9Fe_1@CNFs, Co_2Fe_1@CNFs, Co_1Fe_2@CNFs and Co_1Fe_9@CNFs. For the synthesis of CNF, only needed to remove the metal nitrates, other conditions were the same as above.

Material characterizations： X-ray diffraction (XRD) analysis of the samples was performed by Rigaku Ultima IV X-ray diffractometer with Cu Kα radiation. The sample morphology was photographed by ZEISS Gemini SEM 360 scanning electron microscope. The acceleration voltage was 3 kV during topography shooting and 15 kV during energy spectrum mapping shooting. The detector is SE2 secondary electronic detector. The transmission electron microscopy (TEM) and high-resolution TEM (HRTEM) images of sample were obtained using JEOL JEM-200F equipment with the accelerating voltage of 300 kV. The ion chromatography (IC) was tested by Thermo Scientific ICS-900. The Differential Electrochemical Mass Spectrometry (DEMS) measurements were performed on the Linglu QAS 100.The Inductively Coupled Plasma Optical Emission Spectrometer (ICP-OES) was tested by Agilent 5110.

Working electrode preparation: 5 mg of catalyst were grinded into powder and

added into a mixed solution containing 655 μL of ethanol, 325 μL of deionized water and 20 μL of 5 wt% Nafion solution, followed by 30 min ultrasonic dispersion to form a homogeneous suspension. Then, 20 μL of such suspension was dropped on carbon paper (CP, 1×1 cm^2), and dried at ambient temperature.

Electrochemical measurements: All electrochemical measurements were performed in a hydrogen cell equipped with a Nafion membrane in the middle. The experiments were conducted using a three-electrode system. The working electrode was a carbon sheet coated with the catalyst, the counter electrode was a platinum tablet, and the reference electrode was a Hg/Hgo electrode. The electrolyte for both the anode and cathode was 0.1 M NaOH solution with pH=13. Sodium nitrate ($NaNO_3$) was added to the high-temperature, purified electrolyte as a nitrogen source.

In 0.1 M NaOH with 0.1 M $NaNO_3$ electrolyte, the voltage of the relative reference electrode (Hg/HgO) was converted into the voltage of the relatively reversible hydrogen electrode (RHE) by formula (1):

$$E(RHE) = 0.0591 \times PH + E\left(\frac{Hg}{HgO}\right) + 0.098V \quad (1)$$

The linear sweep voltammetry (LSV) was performed to compare the presence and absence of nitrate salts in the same electrolyte at a scan rate of 5 mV s^{-1}. Under non-Faradaic current conditions, cyclic voltammetry (CV) experiments were carried out at scan rates of 100 mV s^{-1}, 140 mV s^{-1}, 180 mV s^{-1}, 220 mV s^{-1} and 260 mV s^{-1} in the potential range from –0.05 V to 0.05 V *vs*. Hg/HgO. Electrochemical impedance spectroscopy (EIS) was employed to measure the solution resistance within a frequency

range of 0.1 to 10 kHz.

Determination of ammonia (NH_3): Ammonia produced in the NITRR process was colored by indophenol blue method and detected by the UV-vis spectroscopy. Due to the high concentration of the product, all electrolytes after electrolysis were diluted 20 times before color development. After 1 hour of electrolysis, the electrolyte was diluted 20 times to 2 mL, followed by 2 mL of colorant (containing salicylic acid, sodium citrate and sodium hydroxide), 1 mL of oxidant (0.05 M sodium hypochlorite), and 0.2 mL of catalyst solution (1 wt% sodium nitroferricyanide). Then, they were placed in the dark environment for 2 h, and the UV-vis spectra were measured in the wavelength range of 550 ~ 800 nm. The absorption intensity at 655 nm was substituted into the standard curve to quantify the ammonia yield. Calibration of NH_4Cl standard solutions with different concentrations was carried out, and the fitting curve was calculated as $y=0.4387x+0.0417$. ($R^2=0.999$).

Determination of Nitrite (NO_2^-): The nitrite concentration was measured using the Griess reagent. To prepare the Griess reagent, 0.2 g of N-(1-naphthyl) ethyl-enediamine dihydrochloride, 2.0 g of sulfanilamide, and 5.88 mL of phosphoric acid were dissolved in 100 mL of deionized water and stirred thoroughly. This formed the Griess reagent. After electrolysis, the electrolyte was diluted 10 times, and then 1 mL of the Griess reagent and 2 mL of deionized water were added. 1 mL of the diluted electrolyte was taken and allowed to react in the dark at room temperature for 20 minutes, during which the solution developed a magenta color. The absorbance was measured using a UV-Vis spectrophotometer in the 400 ~ 650 nm range, and the

absorbance at 540 nm was recorded. The nitrite concentration was determined by comparing the absorbance value at 540 nm to a standard calibration curve. The calibration of $NaNO_2$ standard solutions with different concentrations was carried out, and the fitting curve was calculated as y=0.2124x+0.0208. (R^2=0.999).

Detection of hydrogen (H_2): In the NITRR process, there is a competing reaction, the Hydrogen Evolution Reaction (HER), occurring at the cathode. Since H_2 is a product of the HER, it can be detected by passing the electrolysis products into a gas chromatograph (GC) through the cathode chamber. To minimize experimental errors caused by differences in the thermal conductivity of gases, nitrogen was used as the carrier gas for the chromatograph. Nitrogen was introduced into the cathode electrolyte at a flow rate of 20 mL min^{-1}, and the GC collected the gas produced by the reaction in the cathode chamber every 5 minutes. By integrating the characteristic peak of hydrogen detected by the thermal conductivity detector (TCD), the concentration of hydrogen can be determined.

Calculations of faradaic efficiency (FE) and yield rate:

The FE of NH_3 is calculated by equation (2):

$$NH_3\ FE = \frac{8 \times F \times c(NH_3) \times V}{17 \times Q} \times 100\%$$

(2)

The FE of NO_2^- is calculated by equation (3):

$$NO_2^-\ FE = \frac{2 \times F \times c(NO_2^- \times V)}{46 \times Q} \times 100\%$$

(3)

The yield of NH_3 is calculated by equation (4):

$$NH_3\ yield\left(\mu g\ h^{-1}\ mg_{cat.}^{-1}\right) = \frac{c(NH_3) \times V}{t \times m_{cat.}} \quad (4)$$

The yield of NH_3 is calculated by equation (5):

$$NO_2^-\ yield\left(\mu g\ h^{-1}\ mg_{cat.}^{-1}\right) = \frac{c(NO_2^-) \times V}{t \times m_{cat.}} \quad (5)$$

The concentration of H_2 is measured by GC and TCD. The volume mole number n can be calculated according to formula (6):

$$n = \frac{P \times V(H_2)}{RT} \quad (6)$$

The corresponding FE of H_2 can be calculated by equation (7):

$$H_2FE = \frac{2 \times F \times n}{Q} \times 100\% \quad (7)$$

c (mg h^{-1} $mg^{-1}_{cat.}$): the measured NH_3/ NO_2^- concentration. V: the volume of electrolyte in the cathode chamber. t: the time for which the potential is applied. F: Faraday constant (F=96485 C mol^{-1}). $m_{cat.}$: the mass of catalyst loaded on the working electrode. Q: the charge applied. P: the standard atmospheric pressure. V(H_2): volume of hydrogen generated by GC test. R: the universal gas constant. T: the reaction temperature.

Differential Electrochemical Mass Spectrometry (DEMS) measurements:

The 0.1 M $NaNO_3^-$ based NaOH solution was pumped into the electrochemical cell using a peristaltic pump. Prior to and during the DEMS test, argon (Ar) was continuously bubbled into the electrolyte at a flow rate of 0.8 mL/min. A carbon paper coated with catalysts electrocatalyst was used as the working electrode, a platinum wire

as the counter electrode, and Hg/HgO as the reference electrode. The experiment began with a linear sweep voltammetry (LSV) scan from 0.8 V vs. RHE to –1.2 V vs. RHE at a scan rate of 10 mV s^{-1}. The scan continued until the baseline stabilized, and then the corresponding mass signals were collected. After the electrochemical test, once the mass signal returned to the baseline, the next cycle was performed under the same conditions to avoid any experimental errors. The DEMS test was completed after four cycles.

Computational methods

First-principles calculations were performed within the density functional theory framework [1]. The projector-augmented wave (PAW) method [2, 3] and the generalized gradient approximation (GGA) [4] for the exchange-correlation energy functional, as implemented in the Vienna ab initio simulation package (VASP) [5-8] were used. The GGA calculation was performed with the Perdew-Burke-Ernzerhof (PBE) [9] exchange-correlation potential. Considered long-range interaction between molecules/intermediates and surface, Van der Waals interactions were considered using DFT-D3 correlation [10]. A combined supercell slab model was built to simulate the surface of the catalyst. To avoid effects come from other slabs, a vacuum of 15 Å was added along z direction. The convergence criterion of geometry relaxation was set to 0.03 eV·$Å^{-1}$ in force on each atom. The energy cutoff for plane wave-basis was set to 600 eV. The K points were sampled with 3×3×1 by Monkhorst-Pack method.

The effect of solvation was simulated by the polarizable continuum models (PCM)[11]. The change in free energy (ΔG) of per reaction step is calculated as follows[12]:

$$\Delta G = \Delta E + \Delta ZPE - T\cdot\Delta S + \Delta G_U + \Delta G_{pH}$$

where ΔE is the change of the total reaction energy obtained from DFT calculation, ΔZPE the change of the zero-point energy, T the temperature (300 K), and ΔS the change of the entropy. $\Delta G_U = -eU$, where U is the potential at the electrode and e is the transferred charge. $\Delta G_{pH} = k_B \cdot T \times \ln 10 \times pH$, where k_B is the Boltzmann constant and

T = 300 K. In this work, the value of pH was derived from experimentally determined pH values.

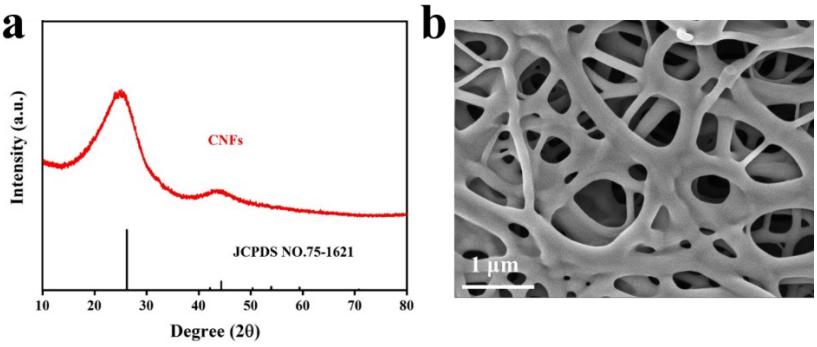

Fig. S1. (a) XRD pattern and (b) SEM image of CNFs.

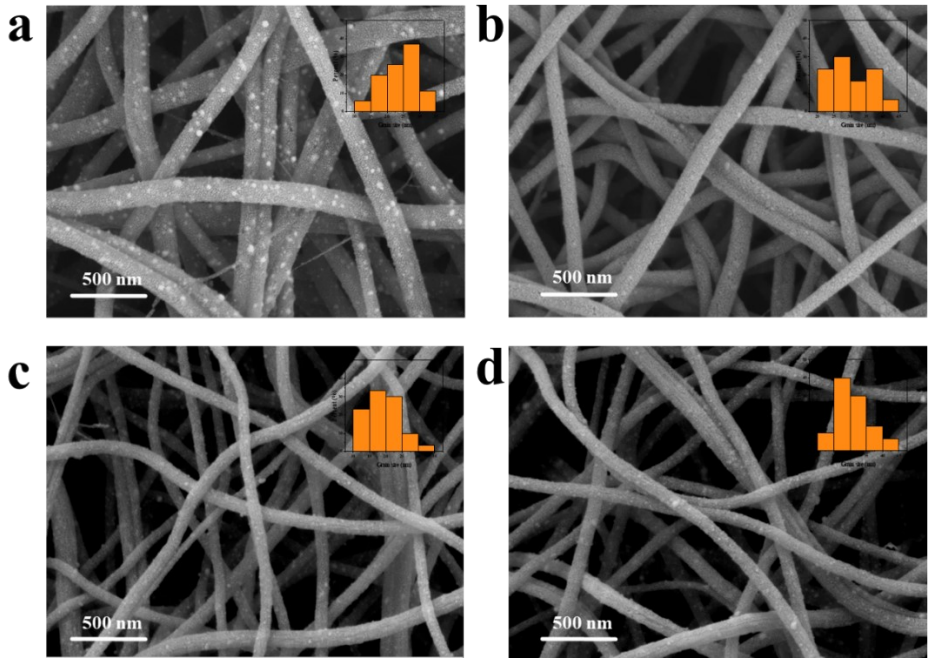

Fig. S2. (a) SEM image of Co_2Fe_1@CNFs, (b) Co_1Fe_1@CNFs, (c) Co_1Fe_2@CNFs and (d) Co_1Fe_9@CNFs.

a

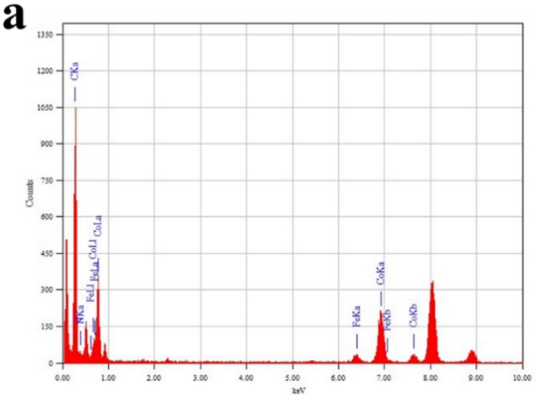

b

Elements	wt%	atomic percent(%)
C	75.18	93.52
N	0.18	0.19
Fe	2.51	0.67
Co	22.13	5.6
Total	100.00	100.00

Fig. S3. EDX spectrum of Co_9Fe_1@CNFs.

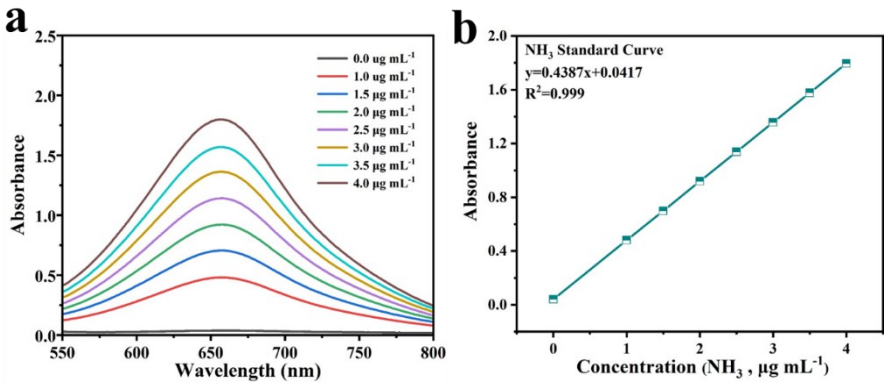

Fig. S4. (a) UV-vis absorption spectra of different concentrations of NH_3 stained with indophenol blue and (b) the corresponding calibration curve in 0.1 M NaOH.

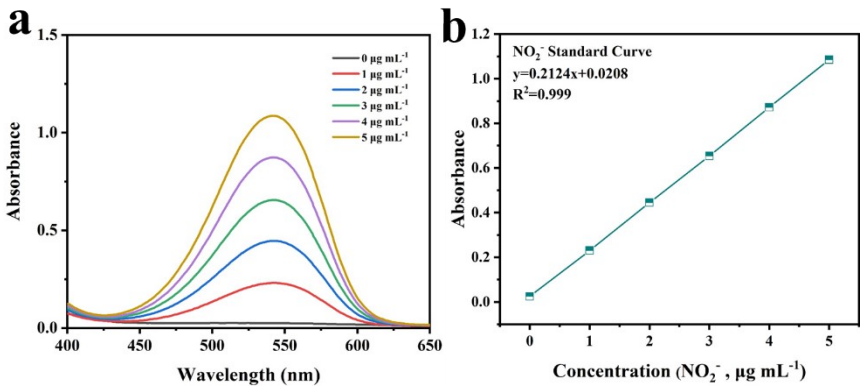

Fig. S5. (a) UV-vis absorption spectra and (b) corresponding calibration curve of NO_2^-.

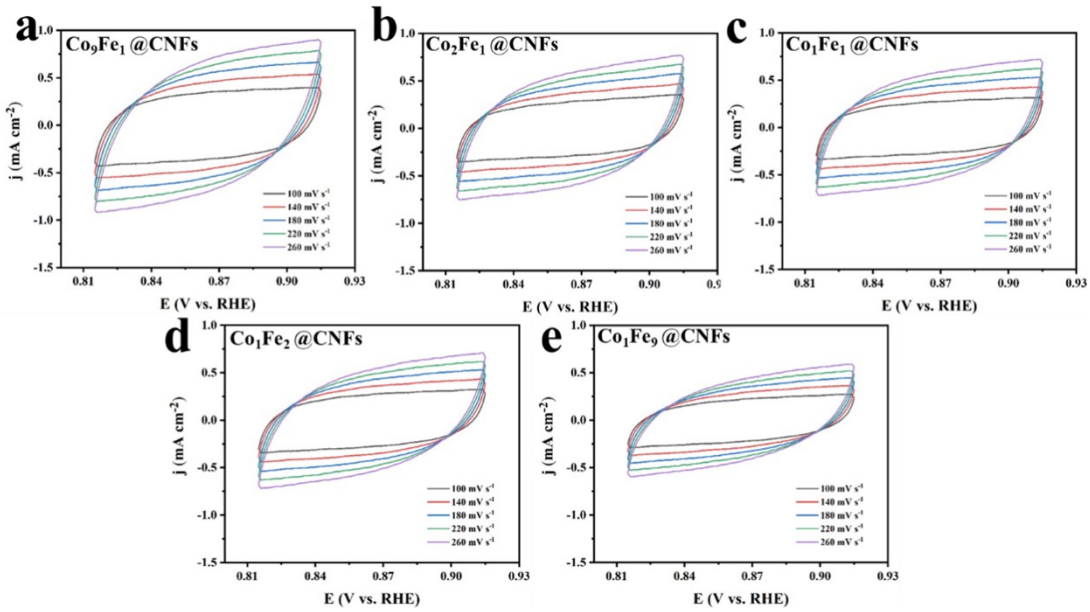

Fig. S6. CV curves of different scan rates of (a) Co_9Fe_1@CNFs, (b) Co_2Fe_1@CNFs, (c) Co_1Fe_1@CNFs, (d) Co_1Fe_2@CNFs and (e) Co_1Fe_9@CNFs at 300 K.

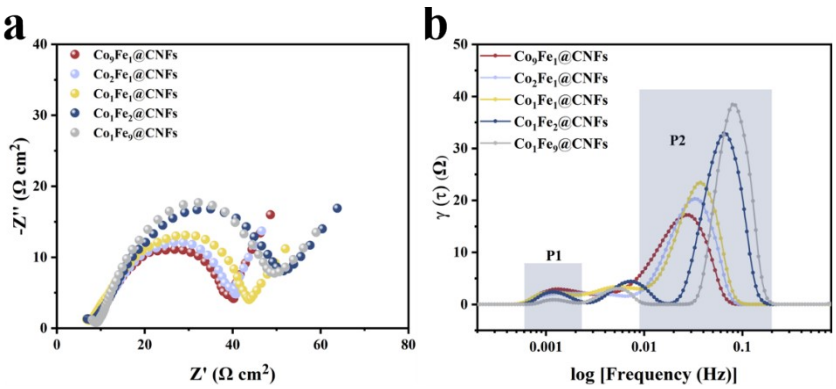

Fig. S7. (a) EIS Nyquist plots at 300 K. (b) DRT analysis of electrochemical impedance spectra.

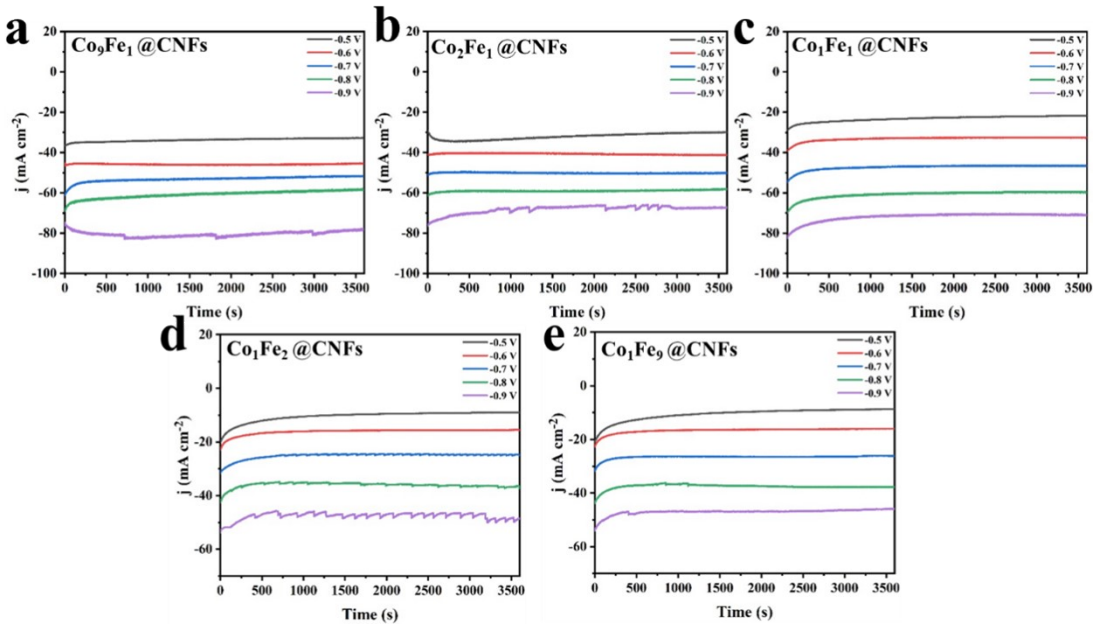

Figure S8. i-t curves for 1 h of (a) Co_9Fe_1@CNFs, (b) Co_2Fe_1@CNFs, (c) Co_1Fe_1@CNFs, (d) Co_1Fe_2@CNFs and (e) Co_1Fe_9@CNFs at 300 K.

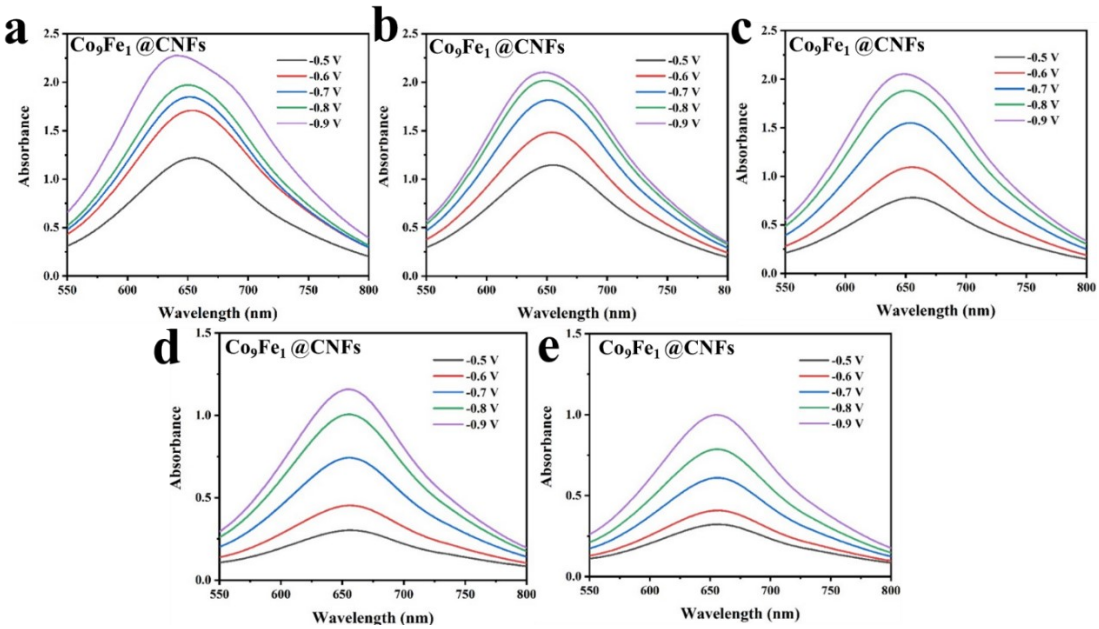

Figure S9. UV-vis absorption spectra at various potentials (–0.5 V to –0.9 V vs. RHE diluted 20 times) of (a) Co_9Fe_1@CNFs, (b) Co_2Fe_1@CNFs, (c) Co_1Fe_1@CNFs, (d) Co_1Fe_2@CNFs and (e) Co_1Fe_9@CNFs at 300 K.

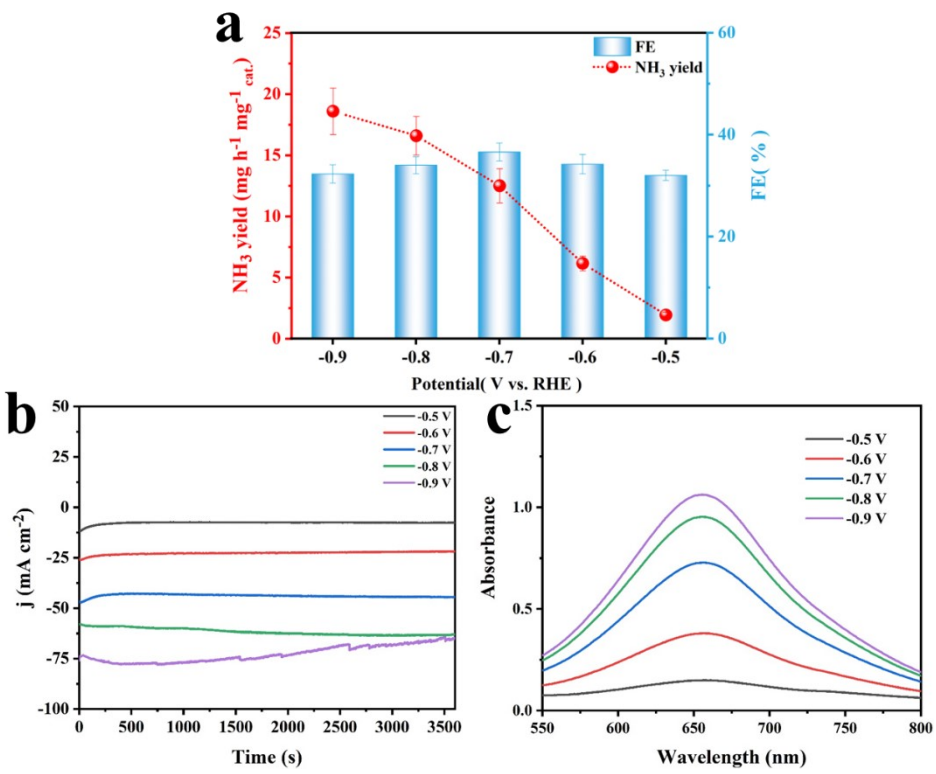

Fig. S10. (a) NH_3 yield and FEs of CNFs at different applied potentials. (b) i-t curves for 1 h and (c) UV-vis absorption spectra at various potentials (–0.5 V to –0.9 V vs. RHE are diluted 20 times) of CNFs at 300 K.

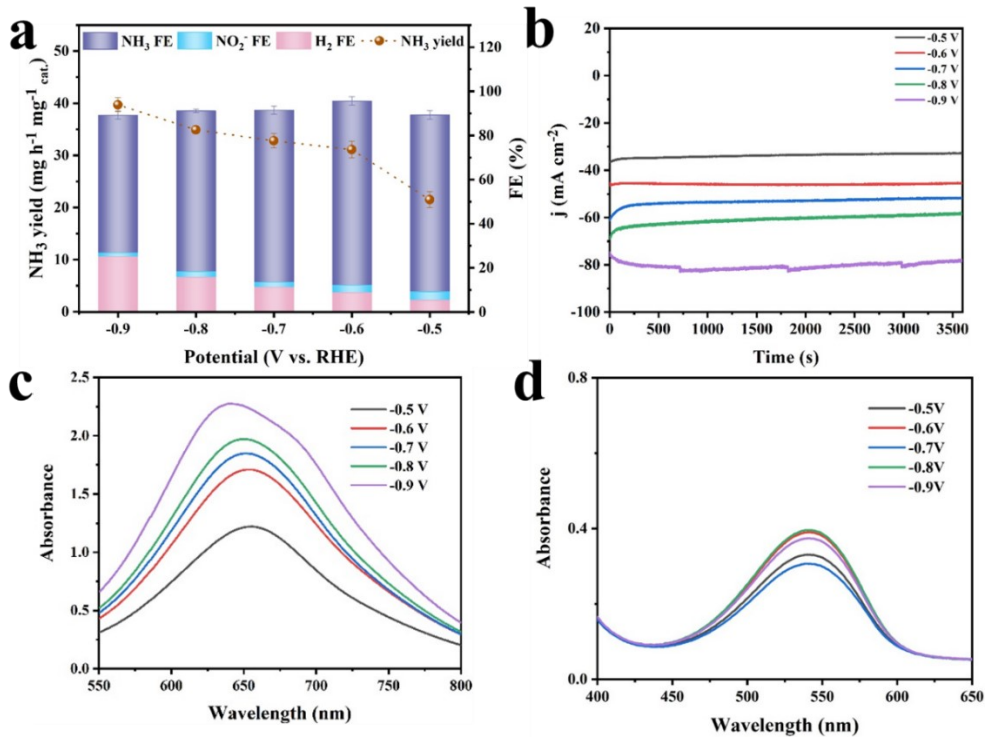

Figure S11. (a) FEs of three reduction products and NH_3 yields of Co_9Fe_1@CNFs at different potentials. (b) i-t curves for 1 h of Co_9Fe_1@CNFs at 300 K. UV-vis absorption spectra for (c) NH_3 yield and (d) NO_2^- yield of Co_9Fe_1@CNFs in NaOH with 0.1 M NO_3^-.

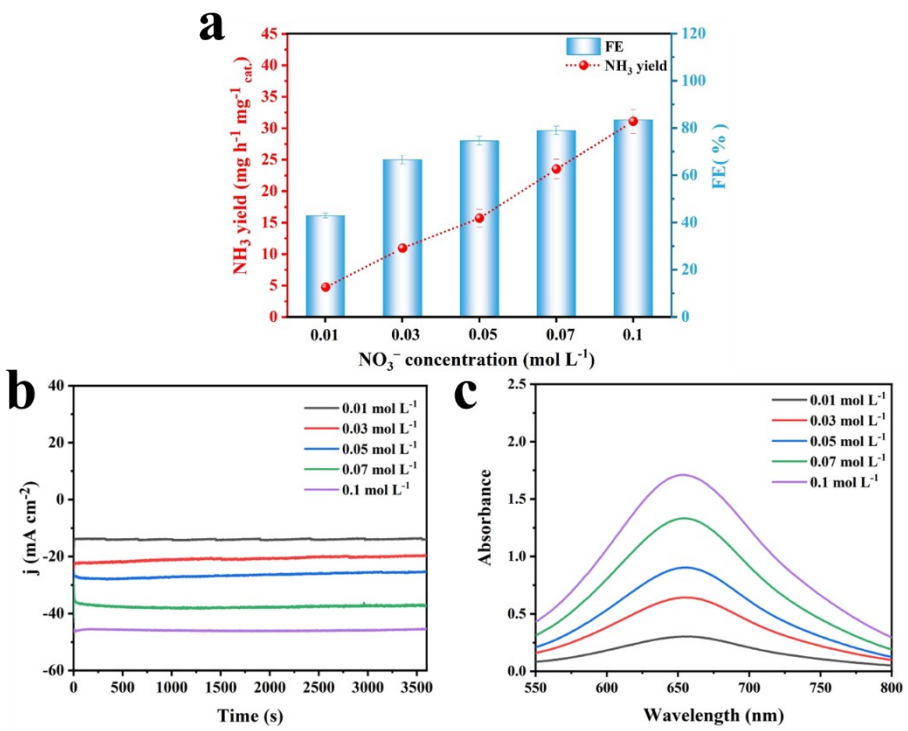

Fig. S12. (a) NH_3 yield and FEs of Co_9Fe_1@CNFs in electrolytes of five different NO_3^- concentrations at −0.6 V vs. RHE. (b) i-t curves for 1 h and (c) UV-vis absorption spectra at various NO_3^- concentrations (0.01-0.1M) of Co_9Fe_1@CNFs at 300 K.

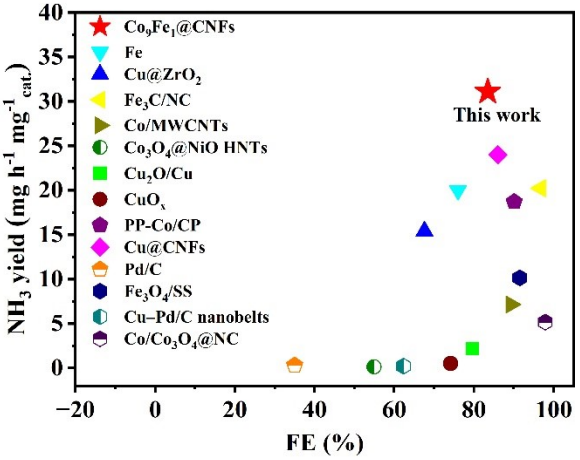

Fig. S13. Comparison of Co_9Fe_1@CNFs with some reported catalysts.

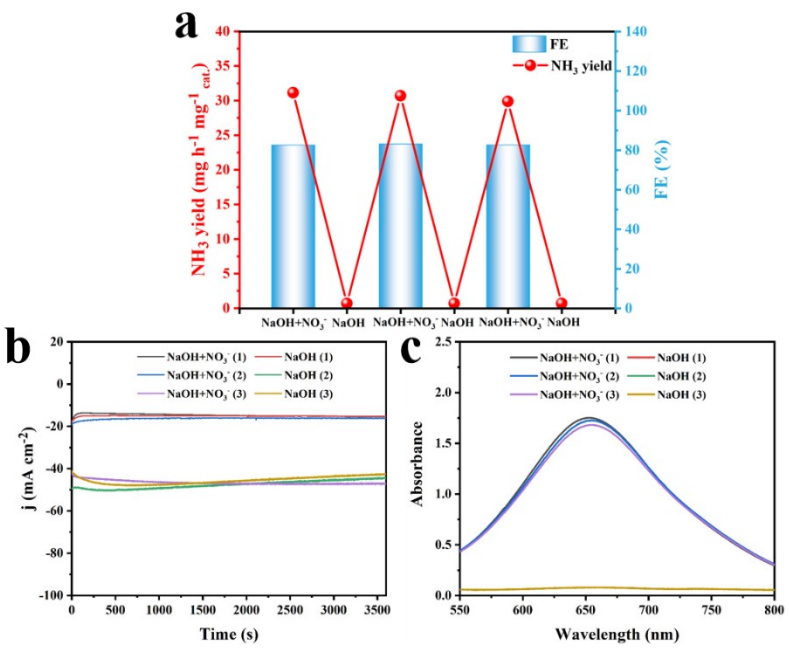

Fig. S14. (a) Repeated testing of 0.1 M NaOH electrolyte with and without NO_3^-. (b) i-t curves and (c) UV-vis absorption spectra of NH_3 with alternating 1 h cycles in the NaOH electrolyte with and without NO_3^- of Co_9Fe_1@CNFs at 300 K.

.

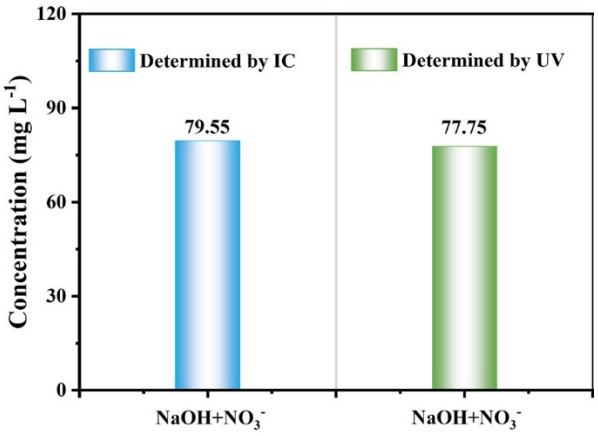

Fig. S15. The NH_3 yield rate detected using the IC method and UV method after 1 h electrolysis in 0.1 M NaOH with 0.1 M NO_3^- at –0.6 V over Co_9Fe_1@CNFs.

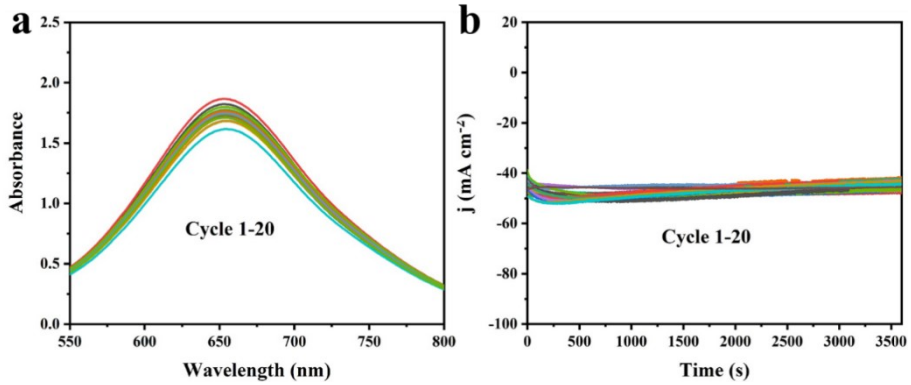

Fig. S16. (a) i-t curves for 1 h and (b) UV-vis absorption spectra of NH_3 of cycling test for Co_9Fe_1@CNFs at 300 K.

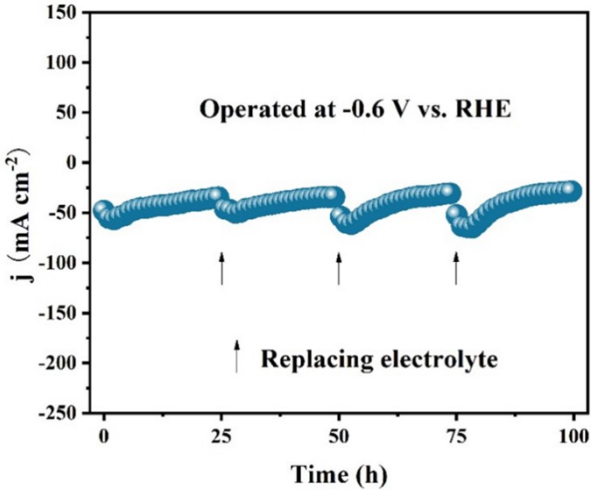

Fig. S17. Stability test on Co_9Fe_1@CNFs for 100 h electrolysis at 300 K.

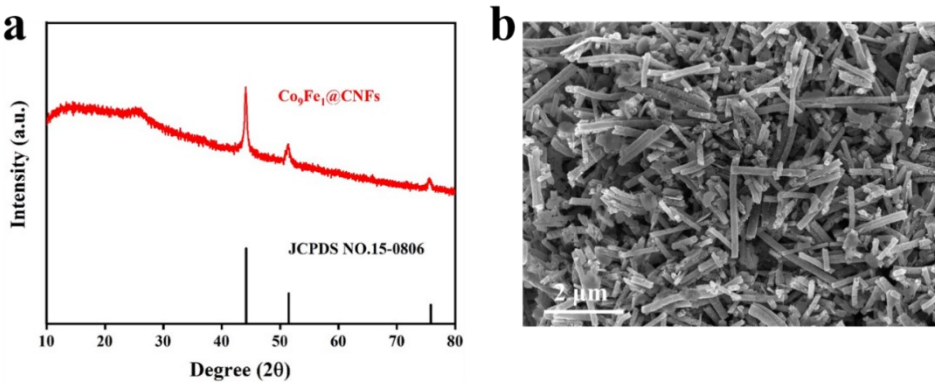

Fig. S18. (a) XRD pattern of Co_9Fe_1@CNFs after calcination. (b) SEM image of Co_9Fe_1@CNFs after calcination.

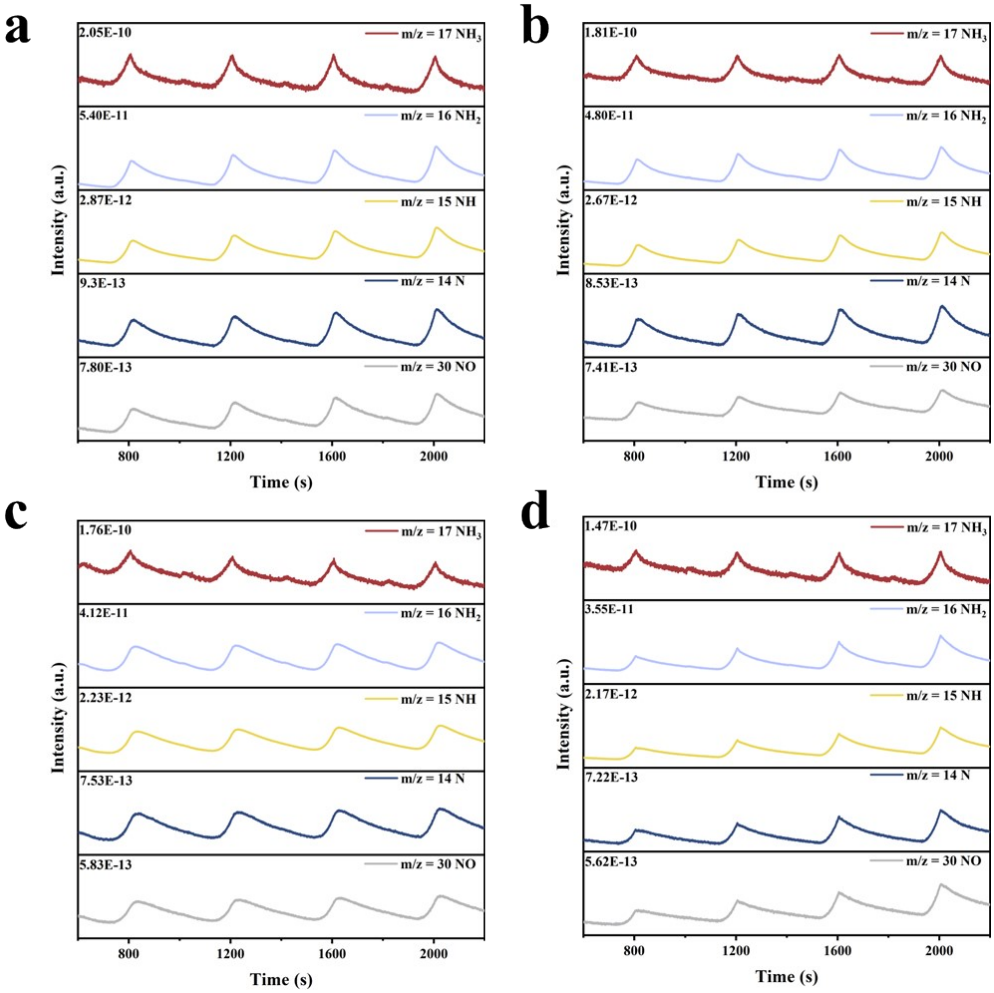

Fig. S19. DEMS tests on (a) Co_2Fe_1@CNFs, (b) Co_1Fe_1@CNFs, (c) Co_1Fe_2@CNFs and (d) Co_1Fe_9@CNFs.

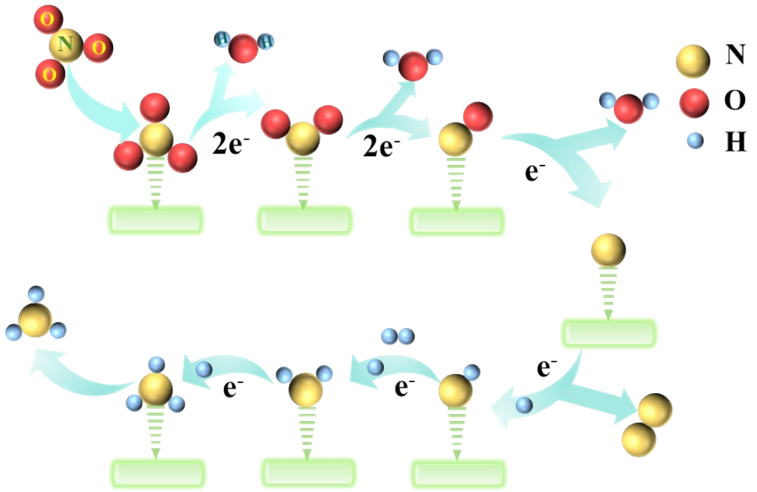

Fig. S20. Schematic diagram of the NO_3RR pathway at the surface of Co_9Fe_1@CNFs.

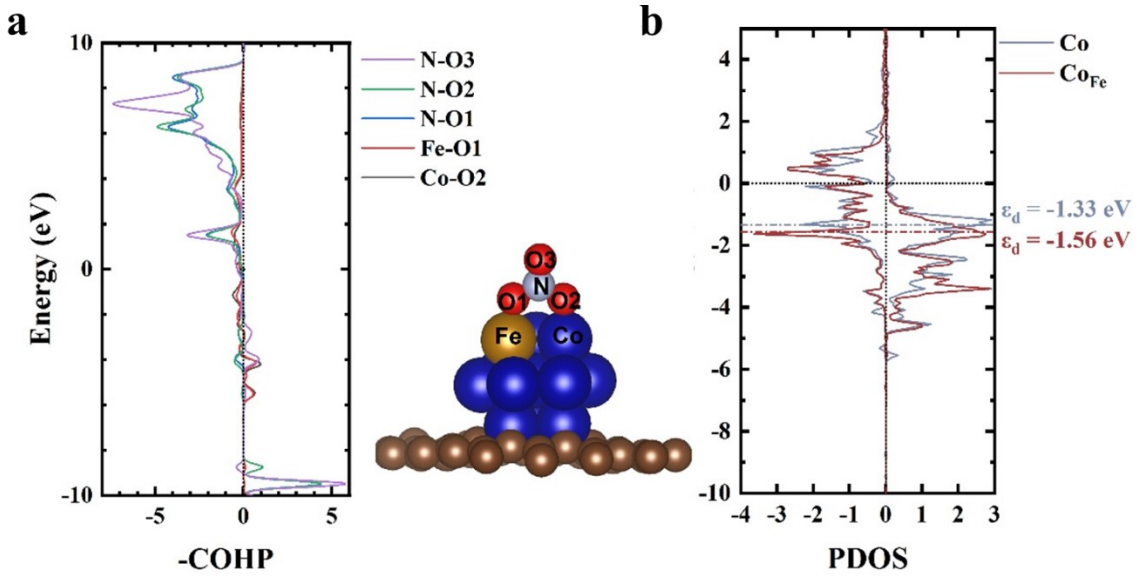

Fig. S21. (a) The COHP of the N-O, Fe-O, and Co-O bonds. (b) The PDOS and the corresponding ε_d of the Co atom.

Table S1. ICP-OES quantitative analysis of the Co_9Fe_1@CNFs catalyst.

Catalysts	Co Element content(wt.%)	Fe Element content(wt.%)	Co:Fe Molar Ratio
Co_9Fe_1@CNFs	19.845	2.070	9.00:1.00

Table S2. Comparison of electrocatalytic NitRR performance for Co_9Fe_1@CNFs with other electrocatalysts under ambient conditions.

Catalysts	Electrolyte	Potential(V)	FE	NH_3 yield	Ref.
Co_9Fe_1@CNFs	**0.1 M NaOH with 0.1 M $NaNO_3$**	**–0.6 V**	**83.50%**	**31.1 mg h^{-1} $mg^{-1}_{cat.}$**	**This work**
Cu@CNFs	0.1 M PBS with 0.1 M $NaNO_3$	–1.2 V	86.38%	24.22 mg h^{-1} $mg^{-1}_{cat.}$	13
Fe	0.50M KNO_3, 0.10 M K_2SO_4	–0.66	76.00%	20 mg h^{-1} $mg^{-1}_{cat.}$	14
Co_3O_4@NiO HNTs	0.5M Na_2SO_4 +200 ppm NO_3^-	–0.70	54.97%	0.12 mg h^{-1} $mg^{-1}_{cat.}$	15
Cu_xO	50 ppm KNO_3+0.1 M KOH^-	–0.25	74.18%	0.449 mg h^{-1} $mg^{-1}_{cat.}$	16
Co/Co_3O_4@NC	0.5M Na_2SO_4 +100 ppm NO_3^-	-0.40	97.90%	5.16 mg h^{-1} $mg^{-1}_{cat.}$	17
Co/MWCNTs	0.1 M KOH +100 mM NO_3^-	–0.50	89.30%	7.41 mg h^{-1} $mg^{-1}_{cat.}$	18
Cu_2O/Cu	1 M KOH + 250 mg L^{-1} NO_3^-	–0.25	79.64%	2.17 mg cm^{-2} h^{-1}	19
Fe_3O_4/SS	0.1 M NaOH + 0.1 M $NaNO_3$	–0.50	91.50%	10.145 mg cm^{-2} h^{-1}	20
Pd/C	0.1 M NaOH + 0.02 M $NaNO_3$	–0.20	35%	0.307 mg h^{-1} $mg^{-1}_{cat.}$	21
Cu@ZrO_2	0.1 M PBS with 0.1 M $NaNO_3^-$	–0.70	67.6%	15.40 mg h^{-1} $mg^{-1}_{cat.}$	22
Cu-Pd/C nanobelts	0.1 M KOH +0.01M KNO_3	–0.40	62.3%	0.221 mg h^{-1} $mg^{-1}_{cat.}$	23
PP-Co/CP	0.1 M NaOH with 0.1 M $NaNO_3$	–0.70	90.1%	18.7 mg h^{-1} $mg^{-1}_{cat.}$	24
Fe3C/NC	0.1 M KOH +75 mM NO_3^-	–0.50	96.70%	20.23 mg h^{-1} $mg^{-1}_{cat.}$	25

Reference:

1. W. Kohn and L. J. Sham, *Phys. Rev.*, 1965, **140**, A1133-1138.
2. P. E. Blöchl, *Phys. Rev. B*, 1994, **50**, 17953.
3. G. Kresse and D. Joubert, *Phys. Rev. B*, 1999, **59**, 1758-1775.
4. J. P. Perdew and Y. Wang, *Phys. Rev. B*, 1992, **45**, 13244-13249.
5. G. Kresse and J. Hafner, *Phys. Rev. B*, 1993, **47**, 558-561.
6. G. Kresse and J. Furthmüller, *Phys. Rev. B*, 1996, **54**, 11169.
7. L. Chen, L. Z. Zhou, H. B. Lu, Y. Q. Zhou, J. L. Huang, J. Wang, Y. Wang, X. L. Yuan and Y. Yao, *Chem. Commun.*, 2020, **56**, 9138-9141.
8. G. Kresse and J. Furthmüller, *Comput. Mater. Sci.*, 1996, **6**, 15-50.
9. J. P. Perdew, K. Burke and M. Ernzerhof, *Phys. Rev. Lett.*, 1996, **77**, 3865-3868.
10. S. Grimme, J. Antony, S. Ehrlich and H. Krieg, *J. Chem. Phys.*, 2010, **132**, 154104.
11. K. Mathew, R. Sundararaman, K. Letchworth-Weaver, T. A. Arias and R. G. Hennig, *J. Chem. Phys.*, 2014, **140**, 084106.
12. J. K. Nørskov, J. Rossmeisl, A. Logadottir, L. Lindqvist, J. R. Kitchin, T. Bligaard and H. Jónsson, *J. Phys. Chem. B*, 2004, **108**, 17886-17892.
13. T. Wang, L. Niu, K. Zhang, Y. Wang, H. guo, X. He, H. Xian and T. Li, *Chem. Commun.*, 2025, **61**, 3532-3535.
14. Z. Wu, M. Karamad, X. Yong, Q. Huang, D. A. Cullen, P. Zhu, C. Xia, Q. Xiao, M. Shakouri, F. Chen, J. Y. Kim, Y. Xia, K. Heck, Y. Hu, M. S. Wong, Q. Li, I. Gates, S. Siahrostami and H. Wang, *Nat. Commun*, 2021, **12**, 2870.
15. Y. Wang, C. Liu, B. Zhang and Y. Yu, Sci. *China Mater.*, 2020, **63**, 2530-2538.
16. J. Geng, S. Ji, H. Xu, C. Zhao, S. Zhang and H. Zhang, *Inorg. Chem. Front.*, 2021, **8**, 5209-5213.
17. L. Zhang, B. Zhang, Y. Hong, Y. You, Y. Zhou, J. Zhan, D. Alonzo Poole Iii and F. Yu, *Small*, 2024, **20**, 2402430.
18. M. Ye, X. Jiang, Y. Zhang, Y. Liu, Y. Liu and L. Zhao, *Nanomaterials*, 2024, **14**, 102.
19. W. Fu, Z. Hu, Y. Zheng, P. Su, Q. Zhang, Y. Jiao and M. Zhou, *Chem. Eng. J.*, 2022, **433**, 133680.
20. X. Fan, L. Xie, J. Liang, Y. Ren, L. Zhang, L. Yue, T. Li, Y. Luo, N. Li, B. Tang, Y. Liu, S. Gao, A. A. Alshehri, Q. Liu, Q. Kong and X. Sun, *Nano Res.*, 2022, **15**, 3050-3055.
21. J. Lim, C. Liu, J. Park, Y. Liu, T. P. Senftle, S. W. Lee and M. C. Hatzell, *ACS Catal.*, 2021, **11**, 7568-7577.
22. J. Xia, H. Du, S. Dong, Y. Luo, Q. Liu, J. S. Chen, H. Guo and T. Li, *Chem. Commun.*, 2022, **58**, 13811-13814.
23. Z. Wang, C. Sun, X. Bai, Z. Wang, X. Yu, X. Tong, Z. Wang, H. Zhang, H. Pang, L. Zhou, W. Wu, Y. Liang, A. Khosla and Z. Zhao, *ACS Appl. Mater. Interfaces*, 2022, **14**, 30969-30978.
24. Q. Chen, J. Liang, Q. Liu, K. Dong, L. Yue, P. Wei, Y. Luo, Q. Liu, N. Li, B. Tang, A. A. Alshehri, M. S. Hamdy, Z. Jiang and X. Sun, *Chem. Commun.*, 2022, **58**, 4259-4262.

25. Y. Wang, L. Zhang, Y. Niu, D. Fang, J. Wang, Q. Su and C. Wang, *Green Chem.*, 2021, **23**, 7594-7608.